論文の内容の要旨

Photo-induced charge transfer in $[Ar\text{-}N_2]^+$ and electron diffraction of CCl_3^+ by ion trap

（イオントラップによる$[Ar\text{-}N_2]^+$の光誘起電荷移動およびCCl_3^+の電子回折）

氏名　鈴木　貴裕

I. Introduction

By trapping molecular ions in a Paul-type quadrupole ion trap, we are able to investigate spectroscopic properties of single ion species as well as unimolecular reaction processes starting from single ion species. When ion complexes $[A\cdots B]^+$ are trapped in an ion trap, its photo-excitation will give us an opportunity to investigate a charge transfer reaction within the complex, leading to two different products, that is, $A + B^+$ and $A^+ + B$. In my thesis study, I investigate the mechanism of intermolecular charge transfer processes in $[Ar\cdots N_2]^+$ induced by intense femtosecond near-IR laser fields by ion-trap time-of-flight (TOF) mass spectrometry and show that non-adiabatic couplings among the potential energy curves of the electronic states play a crucial role in the charge transfer reactions, producing the product pairs of $Ar + N_2^+$ and $Ar^+ + N_2$.

On the other hand, it has been known that geometrical structures of molecular ions can be determined by electron diffraction measurements of molecular ions trapped in a Paul-type quadrupole ion trap and the distances between neighboring nuclei in highly symmetric large size clusters such as C_{60}^+ [1] and Ru_{20}^- [2] were estimated. However, it has been an extremely difficult task to determine geometrical structures of fundamental and small-sized molecular ions by the ion-trap gas electron diffraction method because the density of the molecular ions in an ion trap could not be higher than 10^7 molecules/cm^3, which is comparable with the density of background gas species in a vacuum chamber. In my thesis study, I developed an apparatus of an ion-trap electron diffraction and succeeded in recording an electron diffraction pattern of CCl_3^+ generated by dissociative ionization of CCl_4. I was found from the analysis of the diffraction pattern that the geometrical structures are consistent with those obtained by the previous theoretical predictions.

II. Photo-induced charge transfer in $[Ar\cdots N_2]^+$

The electronic ground state of $[Ar\cdots N_2]^+$, having the electron configuration of $Ar(^1S)\cdots N_2^+(X\ ^2\Sigma_g^+)$ and the first and second electronically excited states of $[Ar\cdots N_2]^+$, having the electron configuration of $Ar^+(^2P_{3/2})\cdots N_2(X^1\Sigma_g^+)$ and $Ar^+(^2P_{1/2})\cdots N_2(X^1\Sigma_g^+)$, are strongly mixed in the molecular domain as represented by the overlapping potential energy curves shown in Fig. 1. It has been reported [4,5] that, after the irradiation of visible and UV laser pulses, $[Ar\cdots N_2]^+$ is photodissociated through the two pathways via the first electronically excited state of $[Ar\cdots N_2]^+$:

$$Ar^+(^2P_{3/2})\cdots N_2\ (X^1\Sigma_g^+) \rightarrow Ar^+(^2P_{3/2}) + N_2\ (X^1\Sigma_g^+), \quad (1)$$

$$Ar^+(^2P_{3/2})\cdots N_2\ (X^1\Sigma_g^+) \rightarrow Ar(^1S) + N_2^+(X^2\Sigma_g^+) \quad (2)$$

and that the yield ratio of the charge transfer pathway, γ, defined as

$$\gamma = \frac{I(N_2^+)}{I(Ar^+) + I(N_2^+)} \qquad (3)$$

is in the range of $\gamma = 0.15 \sim 0.25$ when the wavelength of the laser pulses is in the range of 650~270 nm, where $I(Ar^+)$ denotes the yield of Pathway (1) and $I(N_2^+)$ denotes the yield of Pathway (2).

In my thesis study, $[Ar\cdots N_2]^+$, prepared selectively in the Paul-type quadrupole ion trap, is irradiated with ultrashort near-IR (800 nm) laser pulses, and the resultant fragment on species are detected by time-of-flight mass spectrometry. On the basis of the excitation energy dependence of γ, the mechanism of the charge transfer reaction processes is investigated.

The $[Ar\cdots N_2]^+$ complexes formed by the collisions of Ar^+ and N_2^+, which are generated through the multiphoton ionization by the irradiation of femtosecond near-IR intense laser pulses (λ = 800 nm, Δt = 40 fs, I = 1.9-3.1×10^{14} W/cm^2, 5 kHz), with neutral Ar and N_2 are exclusively stored in the ion trap by the stored waveform inverse Fourier transform (SWIFT) method [6]. The trapped $[Ar\cdots N_2]^+$ complexes are irradiated with the femtosecond intense laser pulses, and immediately after the irradiation, the fragment ions, Ar^+ and N_2^+, and the remaining $[Ar\cdots N_2]^+$ complexes are extracted by the pulsed voltage applied to the cap electrodes of the ion trap into the TOF tube for the mass resolved ion detection. From the yield of the Ar^+ originating from Pathway (1) and that of the N_2^+ signals originating from Pathway (2), γ is determined to be $\gamma = 0.62(2)$.

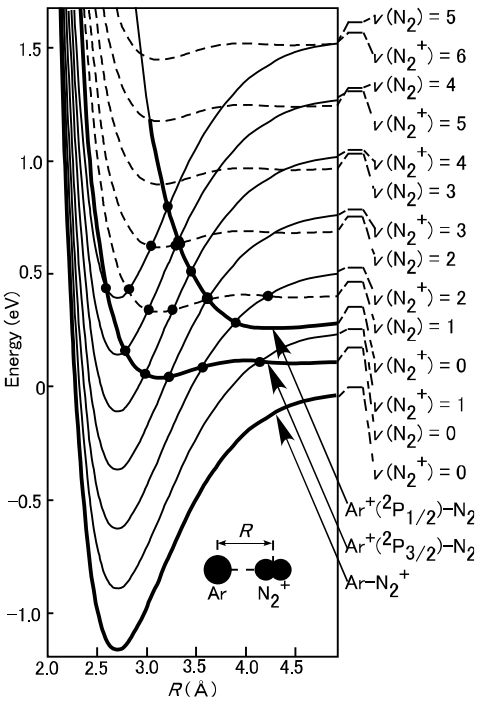

Fig. 1. The potential energy curves of the low-lying electronic states of $[Ar\cdots N_2]^+$ in the linear geometry drawn based on Ref. 3, as a function of the distance R.

As shown in Fig. 2, this γ value is found to be about three times as large as the γ values obtained in the previous studies [4,5] in which the excitation photon energies are higher than 1.91 eV. In order to interpret the excitation photon energy dependence of γ, I performed numerical simulations of the statistical population transfer through the potential crossings using the Landau–Zener–Stückelberg (LZS) model [7-9]. The broken line in Fig. 2 is the result of the numerical simulation of the yield ratio of N_2^+ as a function of the excitation photon energy. In the larger photon energy ($h\nu$ > 1.91 eV), the yield ratio of N_2^+ is in good agreement with the previous experimental results. However, there is a significant discrepancy between the results obtained by the numerical simulation and the experimental result at $h\nu$ = 1.55 eV recorded in the present study. In order to explain the discrepancy, I included the dissociation processes via the intramolecular vibrational energy transfer occurring on the potential energy curve correlating with $Ar + N_2^+$ ($v \geq 1$). The solid line in Fig. 2 is the result of the numerical simulation, exhibiting a good agreement with the experimental result at $h\nu$ = 1.55 eV, confirming that the vibrational energy stored in N_2^+ is transferred to the motion along the dissociation coordinate, that is, the efficient V-T energy transfer proceeds.

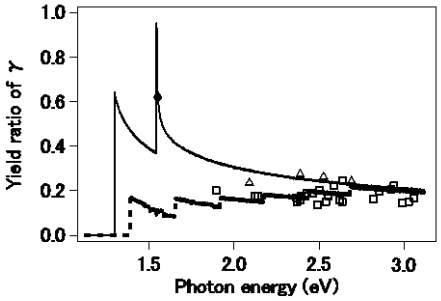

Fig. 2. The yield ratio of N_2^+ as a function of the excitation photon energy calculated by the LZS model (broken line) and the V-T energy transfer model (solid line). circle: present study, open triangles: Ref. 4, and open squares: Ref. 5.

III. Determination of geometrical structure of CCl_3^+

A schematic of the experimental setup of the ion-trap electron diffraction is shown in Fig. 3. The apparatus is composed of a 20 keV electron gun, a Paul-type ion trap, a two-dimensional delay-line detector (DLD) having a central hole (6.4 mmϕ), a pulsed valve (200 Hz). From the pulsed valve, a sample gas (CCl_4) is injected into the ion trap and CCl_3^+ is generated by dissociative ionization induced by a near-IR femtosecond laser pulse (5 kHz, λ = 800 nm, Δt = 40 fs, $I = 8.0\times10^{14}$ W/cm^2). The generated CCl_3^+, which is mass-selectively trapped in the center of the ion trap, is irradiated with an electron beam accelerated to 20 keV. The electron scattering signals are detected by DLD and unscattered electrons, passing through the central hole of the DLD, are trapped by a Faraday cup. In order to reduce background signals originating from stray electrons, a diaphragm with a stainless steel tube (4 mmϕ) is placed between the DLD and the ion trap and two Neodymium magnets are placed closed to the Faraday trap. Owing to the reduction of the background electron signals, it became possible to detect electrons scattered by trapped CCl_3^+ with a count rate of 20 cps.

In Fig. 4, the angular distribution of the scattered electrons, $I(s)$, is shown with red dots as a function of the scattering parameter s defined as $s = \frac{4\pi}{\lambda}\sin\frac{\theta}{2}$, where λ denotes the de Broglie wavelength of electrons and θ denotes the scattering angle. The thin solid curve is a smooth background curve, $I_B(s)$, drawn so that the molecular scattering curve, $sM(s)$, can be extracted, where $sM(s)$ is defined as $(I(s)- I_B(s))/ I_B(s)$. The resulting molecular scattering curve is shown in Fig. 5 with dots. The dotted curve is $sM(s)$ calculated using the structural parameters of r_e(C-Cl) = 1.6501 Å, r_e(Cl···Cl) = 2.8581 Å obtained by theoretical MO calculations [10]. In the calculation of $sM(s)$, it was assumed that takes planer geometry and the mean amplitudes of these atom pairs are 0.12 Å. The good agreement between the observed $sM(s)$ and the theoretical $sM(s)$ show that geometrical structures of molecular ions can be determined with high precision by the ion-trap electron diffraction apparatus.

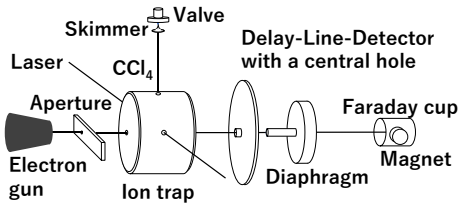

Fig. 3. Schematic of the ion-trap electron diffraction apparatus

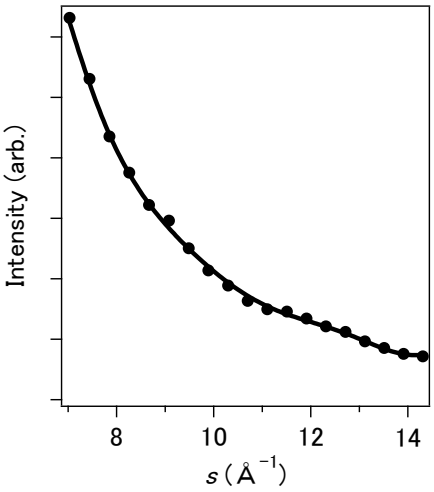

Fig. 4. The recorded electron scattering intensity $I(s)$ (dots) as a function of s and the background curve $I_B(s)$ (solid line).

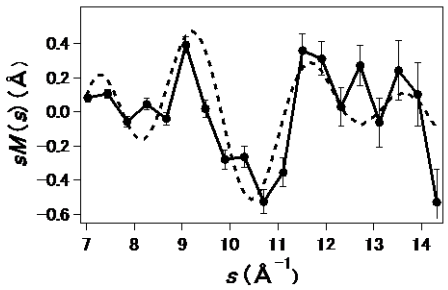

Fig. 5. The recorded (dots) and calculated (broken line) molecular scattering intensities, $sM(s)$, of CCl_3^+.

References

[1] M. Maier-Borst, D. B. Cameron, M. Rokni, J. H. Parks, *Phys. Rev. A* **59,** R3162 (1999).

[2] E. Waldt, A. S. Hehn, R. Ahlrichs, M. M. Kappes, D. Schooss, *J. Chem. Phys.* **142,** R3162 (2015).

[3] R. Candori, S. Cavalli, F. Pirani, A. Volpi, D. Cappelletti, P. Tosi, D. Bassi, *J. Chem. Phys*. **115**, 8888 (2001).

[4] H.-S. Kim, M. T. Bowers, *J. Chem. Phys.* **93**, 1158 (1990).

[5] T. F. Magnera, J. Michl, *Chem. Phys. Lett.* **192**, 99 (1992).

[6] S. Guan, A. G. Marshall, *Int. J. Mass Spectrom. Ion Processes* **157-158**, 5 (1996).

[7] D. Landau, *Phys. Z. Soviet* **2**, 46 (1932).

[8] Zener, *Proc. R. Soc. London, Ser. A* **137**, 696 (1932).

[9] E. G. Stückelberg, *Helv. Phys. Acta* **5**, 369 (1932).

[10] M. Horn, P. Botschwina, *Chem. Phys. Lett.* **228**, 259 (1994).